

# A general variational approach for computing rovibrational resonances of polyatomic molecules. Application to the weakly bound $\text{H}_2\text{He}^+$ and $\text{H}_2 \cdot \text{CO}$ systems

Dóra Papp, Tamás Szidarovszky, and Attila G. Császár

Citation: *The Journal of Chemical Physics* **147**, 094106 (2017); doi: 10.1063/1.5000680

View online: <http://dx.doi.org/10.1063/1.5000680>

View Table of Contents: <http://aip.scitation.org/toc/jcp/147/9>

Published by the [American Institute of Physics](#)

---

## Articles you may be interested in

[A coherent discrete variable representation method on a sphere](#)

*The Journal of Chemical Physics* **147**, 094101 (2017); 10.1063/1.4996891

[Perspective: Computing \(ro-\)vibrational spectra of molecules with more than four atoms](#)

*The Journal of Chemical Physics* **146**, 120902 (2017); 10.1063/1.4979117

[Efficient molecular density functional theory using generalized spherical harmonics expansions](#)

*The Journal of Chemical Physics* **147**, 094107 (2017); 10.1063/1.4994281

[Ro-vibronic transition intensities for triatomic molecules from the exact kinetic energy operator; electronic spectrum for the  \$\tilde{C} 1B\_2 \leftarrow \tilde{X} 1A\_1\$  transition in  \$\text{SO}\_2\$](#)

*The Journal of Chemical Physics* **147**, 094305 (2017); 10.1063/1.4986943

[Complete active space configuration interaction from state-averaged configuration interaction singles natural orbitals: Analytic first derivatives and derivative coupling vectors](#)

*The Journal of Chemical Physics* **147**, 094104 (2017); 10.1063/1.5000476

[Dynamical pruning of the multiconfiguration time-dependent Hartree \(DP-MCTDH\) method: An efficient approach for multidimensional quantum dynamics](#)

*The Journal of Chemical Physics* **147**, 044103 (2017); 10.1063/1.4993219

---



**COMPLETELY  
REDESIGNED!**

**PHYSICS  
TODAY**

*Physics Today* Buyer's Guide  
Search with a purpose.

# A general variational approach for computing rovibrational resonances of polyatomic molecules. Application to the weakly bound $\text{H}_2\text{He}^+$ and $\text{H}_2\cdot\text{CO}$ systems

Dóra Papp, Tamás Szidarovszky, and Attila G. Császár<sup>a)</sup>

Laboratory of Molecular Structure and Dynamics, Institute of Chemistry, Eötvös Loránd University and MTA-ELTE Complex Chemical Systems Research Group, Pázmány Péter sétány 1/A, H-1117 Budapest, Hungary

(Received 10 April 2017; accepted 17 August 2017; published online 7 September 2017)

The quasi-variational quantum chemical protocol and code GENIUSH [E. Mátyus *et al.*, J. Chem. Phys. **130**, 134112 (2009) and C. Fábri *et al.*, J. Chem. Phys. **134**, 074105 (2011)] has been augmented with the complex absorbing potential (CAP) technique, yielding a method for the determination of rovibrational resonance states. Due to the effective implementation of the CAP technique within GENIUSH, the GENIUSH-CAP code is a powerful tool for the study of important dynamical features of arbitrary-sized molecular systems with arbitrary composition above their first dissociation limit. The GENIUSH-CAP code has been tested and validated on the  $\text{H}_2\text{He}^+$  cation: the computed resonance energies and lifetimes are compared to those obtained with a previously developed triatomic rovibrational resonance-computing code, D<sup>2</sup>FOPI-CCS [T. Szidarovszky and A. G. Császár Mol. Phys. **111**, 2131 (2013)], utilizing the complex coordinate scaling method. A unique feature of the GENIUSH-CAP protocol is that it allows the simple implementation of reduced-dimensional dynamical models. To prove this, resonance energies and lifetimes of the  $\text{H}_2\cdot\text{CO}$  van der Waals complex have been computed utilizing a four-dimensional model (freezing the two monomer stretches), and a related potential energy surface, of the complex. *Published by AIP Publishing.* [<http://dx.doi.org/10.1063/1.5000680>]

## I. INTRODUCTION

A rovibrational resonance state of a molecular system, at least within the realm of the Born–Oppenheimer approximation,<sup>1,2</sup> is a state with a finite lifetime which has sufficient energy to break the molecule into one of its non-interacting subsystems.<sup>3</sup> If the lifetime of the resonance state is longer than the time scale of a spectroscopic measurement, it is straightforward to detect the resonance state via (high-resolution) spectroscopy.<sup>4–8</sup> Resonances can also be defined as states of a target-particle system having lifetimes (considerably) longer than those of a direct collision process.<sup>3</sup> In this case, resonances reveal themselves as sudden local irregularities in the collision cross section, occurring at a certain energy.<sup>9</sup> Resonance, or quasi-bound, states play an important role in molecular spectroscopy and in scattering phenomena, and they are also closely related to the dynamics of chemical reactions,<sup>10–16</sup> including photodissociation processes.<sup>17–19</sup> Note that it has recently been shown that monitoring a quantum scattering resonance in an ionization reaction allows the quantification of the anisotropy of an atom-molecule collision.<sup>20</sup>

Theoretical/computational characterization of resonance states commonly follows one of three strategies. The simplest technique, the so-called stabilization method,<sup>21–23</sup> utilizes standard bound-state (ro)vibrational codes, computes a large number of states above dissociation, and then selects, as resonances, those whose energies show some kind of

stability toward small perturbations in the basis. The second route requires the computation of collision cross sections, from which resonance properties can be extracted,<sup>24</sup> based on the equations of quantum dynamics and scattering theory.<sup>25</sup> Along the third route, one determines resonance states as stationary states of a system above its dissociation threshold and computes resonance energies and lifetimes as the *complex* eigenvalues of a non-Hermitian Hamiltonian of the system.<sup>3,26–29</sup> There are two widely used techniques that follow the third route: the complex absorbing potential (CAP)<sup>26,27,30,31</sup> and the complex coordinate scaling (CCS)<sup>28,29</sup> methods. A considerable advantage of the CAP technique is that it allows the utilization of general  $L^2$  bound-state algorithms.<sup>32–36,38</sup> In fact, the CAP technique is an approximation to complex coordinate scaling,<sup>39</sup> and it involves the addition of a special complex potential to the original real rovibronic Hamiltonian. The CAP approach results in the damping of the resonance wave functions at the asymptotic region of the potential energy surface (PES) and provides approximate resonance eigenvalues and eigenfunctions.<sup>3,26</sup> CCS requires the rotation of the dissociation coordinate of the system on the complex plane, thereby providing the resonance eigenvalues with corresponding square-integrable wave functions.<sup>3,7,28,29</sup> This is a direct method, applicable when the Hamiltonian is given in an analytic form. Analytic Hamiltonians include those with fitted PESs; in this case, one needs to rewrite the PES “subroutine” into complex arithmetic.<sup>7</sup> Both the CAP and the CCS methods have been applied during the past two decades to study molecular resonance states.<sup>7,40–46</sup>

<sup>a)</sup>csaszar@chem.elte.hu

Up to now, mostly triatomic molecules have been subjected to detailed resonance computations; nevertheless, resonances of the four-atomic HOCO system have also been investigated, using simplified models.<sup>47–49</sup> Hernández and Clary<sup>47</sup> identified resonance states of HOCO using the stabilization method in a two-dimensional (2D) model, while later Bowman and co-workers computed HOCO resonance states with the help of the CAP technique, first within a 2D<sup>48</sup> and then a 3D model of the system.<sup>49</sup>

Hereby we present an implementation of the CAP technique in the framework of one of the fourth-age quantum chemical<sup>50</sup> quasi-variational approaches and codes, GENIUSH,<sup>36,38</sup> where GENIUSH stands for a general (GE) code with a numerical (N), internal-coordinate (I), user-specified (US) Hamiltonian (H). Combining GENIUSH with CAP allows the straightforward extension of resonance computations to larger molecular systems. The reason is that GENIUSH was designed<sup>36</sup> to provide a general, black-box-type code capable of computing rovibrational bound states not only in full but also in reduced dimensions, using arbitrary coordinate systems and arbitrary embeddings for arbitrary-sized molecules. In GENIUSH, the Hamiltonian is constructed fully numerically. Augmented with the CAP technique, the GENIUSH-CAP algorithm allows the determination of resonance states of polyatomic molecules, as well as their reduced-dimensional models, fully exploiting all the advantages of the GENIUSH approach. Given an efficient implementation of the GENIUSH-CAP method, a universal code becomes available for the investigation of rovibrational states of polyatomic molecules and complexes above their first dissociation limit.

In what follows, we report our implementation of the GENIUSH-CAP method. Testing of the coding utilized the weakly bound  $\text{H}_2\text{He}^+$  complex, where we compared the GENIUSH-CAP resonance energies and lifetimes to those computed with the previously developed<sup>7</sup>  $\text{D}^2\text{FOPI-CCS}$  code. Note that the  $\text{D}^2\text{FOPI-CCS}$  code is applicable only to triatomic molecules. Then, we determine and analyze in some detail vibrational resonance states of the four-atomic  $\text{H}_2\text{-CO}$  van der Waals complex, employing a four-dimensional (4D, with the rigid monomer approximation both for  $\text{H}_2$  and  $\text{CO}$ ) model of the molecule.

## II. GENIUSH-CAP

The toolchest of the GENIUSH code<sup>36,38,51,52</sup> is augmented in this study with the CAP technique<sup>26,27,53,54</sup> to allow the determination of rovibrational resonance states of full- and reduced-dimensional models of polyatomic molecules. GENIUSH computes rovibrational bound states of polyatomic molecules using a discrete variable representation (DVR)<sup>55–57</sup> of the Hamiltonian, and it employs an iterative Lanczos eigensolver,<sup>58</sup> the implementation employed orthogonalizes the Lanczos vectors every second iteration step,<sup>37</sup> to determine the desired rovibrational eigenstates of the molecule investigated. Due to the numerical construction of not only the potential but also the kinetic energy operator, reduced-dimensional models can be defined simply by fixing the internal coordinates at given values.

The CAP method, as mentioned above, is basically a perturbation of the Hamiltonian with a complex potential, which damps the otherwise diverging resonance eigenfunctions of the system in the asymptotic region of the PES. The augmented Hamiltonian can be written as

$$\hat{H}'(\eta) = \hat{H} - i\eta\hat{W}(R), \quad (1)$$

where  $\hat{H}$  is the original Hamiltonian,  $\eta$  is the CAP-strength parameter,  $i$  is the imaginary unit, and  $\hat{W}(R)$  is a real-valued function of the  $R$  dissociation coordinate, assuming nonzero values at the asymptotic region of the PES. As a consequence of the addition of the CAP, the resonance wave functions start to resemble square-integrable functions.<sup>53,59</sup> This makes it possible to use the  $L^2$  eigenvectors obtained when solving the eigenvalue problem of the original real symmetric Hamiltonian as basis functions during the resonance computations,

$$\Psi_{\text{res}} = \sum_i a_i \Phi_{\text{GEN},i}, \quad (2)$$

where  $a_i \in \mathbb{C}$ ,  $\Psi_{\text{res}}$  is the resonance wave function, and  $\Phi_{\text{GEN},i}$  is the  $i$ th eigenvector with an eigenenergy either below or above the first dissociation asymptote, computed with GENIUSH. Despite the fact that most of the  $\Phi_{\text{GEN},i}$  with energies above the first dissociation limit have no real physical meaning, they serve very well as  $L^2$  basis functions for expanding the wave functions of the resonance states. In GENIUSH, rovibrational eigenstates are obtained as linear combinations of the direct products of DVR vibrational and rotational basis functions,

$$\begin{aligned} &\Phi_{\text{GEN},i}(q^{(1)}, q^{(2)}, \dots, q^{(N)}, \alpha, \beta, \gamma) \\ &= \sum_{kl\dots m} \sum_{K=-J}^J c_{kl\dots m,K}^i \chi_k^{(1)}(q^{(1)}) \\ &\quad \times \chi_l^{(2)}(q^{(2)}) \dots \chi_m^{(N)}(q^{(N)}) C_{JKM}(\alpha, \beta, \gamma), \end{aligned} \quad (3)$$

where  $c_{kl\dots m,K}^i$  are real-valued expansion coefficients,  $q^{(1)}, q^{(2)}, \dots, q^{(N)}$  refer to the  $N$  active coordinates used in the given computation, and  $\chi_k^{(1)}, \chi_l^{(2)}, \dots, \chi_m^{(N)}$  denote the DVR functions associated with each active coordinate.  $C_{JKM}(\alpha, \beta, \gamma)$  refer to the  $2J+1$  orthonormal Wang functions used as rotational basis functions<sup>38</sup> depending on the  $\alpha$ ,  $\beta$ , and  $\gamma$  angles, which define three successive rotations around the three orthogonal axes of the molecule-fixed system ( $J$  is the rotational quantum number).  $K = -J, \dots, +J$  is defined by the projection of the total angular momentum  $\hat{J}$  of the system on the molecule-fixed  $z$ -axis, and  $M = -J, \dots, +J$  is the projection of  $\hat{J}$  on the space-fixed  $Z$ -axis. The matrix elements of the new non-Hermitian Hamiltonian represented in the  $\Phi_{\text{GEN},i}$  eigenvector basis can be obtained as

$$\begin{aligned} H'(\eta)_{ij} &= \langle \Phi_{\text{GEN},i} | \hat{H}'(\eta) | \Phi_{\text{GEN},j} \rangle \\ &= E_i \delta_{ij} - i\eta \langle \Phi_{\text{GEN},i} | \hat{W} | \Phi_{\text{GEN},j} \rangle, \end{aligned} \quad (4)$$

where  $E_i$  is the  $i$ th rovibrational energy, and  $\delta$  is the Kronecker delta symbol. Exploiting the orthogonality of the GENIUSH eigenvectors, we need to determine the matrix elements of the complex potential in the basis of these vectors,

$$W_{ij} = \int_{q_{\min}^{(1)}}^{q_{\max}^{(1)}} \int_{q_{\min}^{(2)}}^{q_{\max}^{(2)}} \cdots \int_{q_{\min}^{(N)}}^{q_{\max}^{(N)}} \sum_{kl\dots m} \sum_{k'l'\dots m'} \sum_{K=-J}^J c_{kl\dots m, K}^i c_{k'l'\dots m', K}^j \chi_k^{(1)}(q^{(1)}) \chi_l^{(2)}(q^{(2)}) \cdots \chi_m^{(N)}(q^{(N)}) \times \hat{W} \chi_{m'}^{(N)}(q^{(N)}) \cdots \chi_{l'}^{(2)}(q^{(2)}) \chi_{k'}^{(1)}(q^{(1)}) dq^{(1)} dq^{(2)} \cdots dq^{(N)} V(q^{(1)} q^{(2)} \cdots q^{(N)}). \quad (5)$$

Since  $\hat{W}$  is independent of the rotation angles, the integration over these variables can be performed trivially: due to the orthonormality of the Wang functions, this results in  $\delta_{KK'}$ .  $V(q^{(1)} q^{(2)} \cdots q^{(N)})$  refers to the volume element of the integration. To evaluate this integral, we employ the Gaussian quadrature method using the  $q_a^{(1)}, q_b^{(2)}, \dots, q_c^{(N)}$  DVR grid points as quadrature points. Thus, we transform this integral to a sum, where advantages of the DVR technique can be exploited,

$$W_{ij} = \sum_{ab\dots c} \sum_{kl\dots m} \sum_{k'l'\dots m'} \sum_{K=-J}^J w_a w_b \cdots w_c c_{kl\dots m, K}^i c_{k'l'\dots m', K}^j \chi_k^{(1)}(q_a^{(1)}) \chi_l^{(2)}(q_b^{(2)}) \cdots \chi_m^{(N)}(q_c^{(N)}) W(q_a, q_b, \dots, q_c) \times \chi_{m'}^{(N)}(q_c^{(N)}) \cdots \chi_{l'}^{(2)}(q_b^{(2)}) \chi_{k'}^{(1)}(q_a^{(1)}), \quad (6)$$

where  $w_a, w_b, \dots, w_c$  are quadrature weights. Using the DVR of the original Hamiltonian implies that<sup>57</sup>

$$\chi_k(q_a) = w_a^{-1/2} \delta_{ka}. \quad (7)$$

Due to Eq. (7), the following simple formula describes the elements of the complex Hamiltonian:

$$H'(\eta)_{ij} = E_i \delta_{ij} - i\eta \sum_{ab\dots c} \sum_{K=-J}^J c_{ab\dots c, K}^i c_{ab\dots c, K}^j \times W(q_a, q_b, \dots, q_c). \quad (8)$$

After building the complex Hamiltonian, it is diagonalized with a direct diagonalization method, invoked from the Lapack++ package.<sup>60</sup> Avoiding the use of an iterative eigensolver is possible due to the relatively small dimension of the matrix. The eigenvalues of the complex Hamiltonian are obtained in the form  $E_0 - i\Gamma/2$ , where  $E_0$  is the resonance position and  $\Gamma^{-1}$  is the lifetime of a resonance state in atomic units.

When varying the  $\eta$  CAP-strength parameter, two error types occur with respect to the exact resonance energy.<sup>26</sup> The first one is due to the modification of the original Hamiltonian of the system, which consequently changes the computed resonance eigenvalues with respect to the exact values. This error can be expressed as a power series in  $\eta$ . The second error emerges due to the use of a finite basis set. The first error naturally increases with increasing  $\eta$ , while the second one decreases. This is due to the fact that if we use a stronger absorbing potential, meaning a larger  $\eta$  value, the resonance wave function obtained is damped more effectively in the asymptotic region and therefore becomes more suitable for an expansion in a basis of  $L^2$  functions. If we determine the eigenvalues of the complex Hamiltonian using a given interval of  $\eta$ , eigenvalue trajectories can be drawn on the complex plane, with each point of the trajectory corresponding to an  $\eta$  value. In these trajectories, a cusp forms where the two errors become similar in magnitude, and this cusp position is the best approximation of the exact resonance eigenvalue.<sup>26,27</sup>

To gain further information about resonance states determined with the GENIUSH-CAP procedure, we developed a tool to visualize the probability densities corresponding to the resonance wave functions. For this, we take the resonance wave

function corresponding to the  $\eta$  value at the cusp and, based on Eqs. (2) and (3), plot

$$\sum_{K=-J}^J \left| \sum_{i=1}^J a_i c_{ab\dots c, K}^i \right|^2 \quad (9)$$

at each DVR grid point along two selected coordinates (the other coordinates are held fixed at certain values).

During GENIUSH-CAP computations, one can change and optimize the following: (1) the range where the CAP is turned on; certain resonance states, depending on the extent of their delocalization, are rather sensitive to this choice; (2) the interval of the  $\eta$  parameter, which usually covers several orders of magnitude; (3) the number of GENIUSH eigenvectors employed as basis functions; (4) the number of  $\eta$  values used during a trajectory computation; and (5) the functional form of the CAP. Our choices are detailed below when we discuss the two applications. Here we make only two remarks. First, in GENIUSH-CAP, the  $\eta$  CAP-strength parameter is distributed according to the function

$$\eta_j(\eta_{\min}, \eta_{\max}, n, j) = \eta_{\min} - 1 + \exp[\log((\eta_{\max} - \eta_{\min}) + 1)j / (n - 1)], \quad (10)$$

where  $\eta_j$  is the  $j$ th value of  $\eta$ ,  $n$  is the number of  $\eta$  values, and  $\eta_{\min}$  and  $\eta_{\max}$  are the minimum and maximum values of the given  $\eta$  interval, respectively. Second, we choose the functional form of the CAP to be a polynomial with an order of 1, 2, 3, and 5, optimized by Poirier and Carrington.<sup>61</sup> Employing different functional forms during test computations proved to have only a minimal effect on the results; thus, in this paper, we only present numerical results obtained via using the highest-order polynomial of Ref. 61.

### III. COMPARING GENIUSH-CAP AND D<sup>2</sup>FOPI-CCS RESULTS: THE TEST CASE OF H<sub>2</sub>He<sup>+</sup>

Our choice of the triatomic H<sub>2</sub>He<sup>+</sup> system as a test system was partially inspired by the desire to test the GENIUSH-CAP code under development against results obtained by another, well-established code, D<sup>2</sup>FOPI-CCS,<sup>7</sup> and partially by the astrophysical importance of and the widespread interest in the dynamical features of this triatomic molecule. H<sub>2</sub>He<sup>+</sup> is known to be a collision complex forming instantaneously during the following reactive scattering processes: H<sub>2</sub><sup>+</sup> + He, H<sub>2</sub>

+ He<sup>+</sup>, and HHe<sup>+</sup> + H.<sup>19</sup> Therefore, detailed knowledge of the resonance states of H<sub>2</sub>He<sup>+</sup> is of fundamental importance, see Ref. 62 and references therein. Additionally, it has been found that resonance states play an important role in the strong-field photodissociation processes of H<sub>2</sub>He<sup>+</sup>.<sup>19</sup>

### A. Computational details

The nuclear motions of the H<sub>2</sub>He<sup>+</sup> complex are represented well by the orthogonal Jacobi coordinates  $r = |\mathbf{r}|$ ,  $R = |\mathbf{R}|$ , and  $\theta$ , where  $\mathbf{r}$  connects the two H atoms,  $\mathbf{R}$  points from the center of mass of the two H atoms to the He atom, and  $\theta$  is the included angle of the previous two vectors. For the nuclear motion computations presented in this paper, the PES of H<sub>2</sub>He<sup>+</sup> was taken from Ref. 63. The refined PES of Ref. 63 features dissociation thresholds of  $D_e = 2732.34$  cm<sup>-1</sup> and  $D_0 = 1775.42$  cm<sup>-1</sup>, and it supports 16 bound vibrational states. The equilibrium structure of the H<sub>2</sub>He<sup>+</sup> complex is linear with  $r_e = 2.07792$  bohrs and  $R_e = 2.96596$  bohrs. During the nuclear-motion computations, the following atomic masses were used:  $m_H = 1.00727647$  u and  $m_{He} = 4.00234755$  u.

In the full-dimensional GENIUSH vibration-only bound-state computations, we use 40 and 200 scaled Laguerre-DVR points along the  $r$  and  $R$  coordinates in the range of [1.0, 5.0] and [0.5, 40.0] bohrs, respectively. On the angular coordinate, we use 40 unscaled Legendre-DVR points in the interval of (0.0, 180.0)°. The convergence of the bound-state energies is better than 0.01 cm<sup>-1</sup> with respect to the number of basis functions being increased by 20% on each coordinate. The resonance eigenvalues, both their real and imaginary parts, are converged to within a few 0.1 cm<sup>-1</sup> (with respect to the case when the number of basis functions on the  $R$  coordinate is increased by 20%); however, this convergence strongly depends on the given resonance. For the GENIUSH-CAP computations, we use 400 vibrational GENIUSH eigenvectors as the basis set and change the minimum value of  $R$ , where the CAP is switched on, between 10 and 35 bohrs, while the  $R_{\max}$  value, where the CAP is switched off, is fixed at 40 bohrs. Further GENIUSH-CAP computations were carried out based on a GENIUSH computation with a maximum  $R$  value of 50 bohrs, using 200 basis functions along  $R$ . In this case, the CAP was switched on between 40 and 50 bohrs, and 1500 GENIUSH eigenvectors were used as a basis for the CAP computation.

As a prerequisite of the D<sup>2</sup>FOPI-CCS<sup>7</sup> computations, bound states of the H<sub>2</sub>He<sup>+</sup> system were also computed with the D<sup>2</sup>FOPI code.<sup>35</sup> For these computations, we employed 40 potential-optimized (PO) spherical-DVR basis functions<sup>35</sup> along the  $r$  coordinate, 180 PO spherical-DVR basis functions along the  $R$  coordinate, and 40 Legendre functions along the  $\theta$  coordinate. The coordinate ranges used in the computations are (0.0, 5.0) bohrs for  $r$ , (0, 40) bohrs for  $R$ , and (0.0, 180.0) for  $\theta$ . In the D<sup>2</sup>FOPI-CCS method, resonance eigenstates were obtained by diagonalizing the complex-coordinate-scaled rovibrational Hamiltonian using different values for the scaling parameter and identifying cusps in the resulting eigenvalue trajectories. Details of this approach can be found in Ref. 7. For constructing the matrix representation of the CCS Hamiltonian, 500 vibrational eigenvectors were used. The bound vibrational energy levels computed with D<sup>2</sup>FOPI

and GENIUSH are the same within numerical accuracy, while the convergence of the D<sup>2</sup>FOPI-CCS resonance energies is between 0.01 cm<sup>-1</sup> and 1 cm<sup>-1</sup>, depending on the resonance state.

### B. Resonances of H<sub>2</sub>He<sup>+</sup>

To validate the GENIUSH-CAP code, resonance energies and lifetimes of the triatomic molecule H<sub>2</sub>He<sup>+</sup>, computed with the newly developed code, have been compared with the corresponding results of the D<sup>2</sup>FOPI-CCS code. Since the CCS method does not involve approximations in determining resonance states (apart from utilizing a finite basis), the D<sup>2</sup>FOPI-CCS protocol provides an adequate test to verify the GENIUSH-CAP approach and the corresponding code.

Comparison of resonance eigenvalues, both their real and imaginary parts, obtained by the two different techniques shows remarkably good agreement, see Table I. Table I lists several long-lived resonance eigenvalues of H<sub>2</sub>He<sup>+</sup> located in the energy interval [ $D_0$ , 3000] cm<sup>-1</sup> and having  $|\Gamma/2| < 1$  cm<sup>-1</sup>. We usually obtain resonance energies from the two different techniques within a few 0.1 cm<sup>-1</sup>, and even the obtained lifetimes usually agree within a factor of two, and even in the worst cases, they are of the same order of magnitude. In Table I, we can spot extremely long-lived states at the energies of 1809.0 and 1832.0 cm<sup>-1</sup>, having several orders of magnitude longer lifetimes than the other resonances in the region. These  $B_2$ -symmetry states, when utilizing the  $C_{2v}(M)$  molecular symmetry (MS) group, are characterized by wave functions antisymmetric along the  $\theta$  coordinate. Within this symmetry, the system can dissociate only into the second lowest dissociation channel, when the H<sub>2</sub><sup>+</sup> product is in its first

TABLE I. Long-lived resonances of the H<sub>2</sub>He<sup>+</sup> complex, both real [Re( $E_{\text{res}}$ ) < 3000 cm<sup>-1</sup>] and imaginary [Im( $E_{\text{res}}$ )] parts (cm<sup>-1</sup>), and the corresponding lifetimes (in ps), obtained both with GENIUSH-CAP and D<sup>2</sup>FOPI-CCS computations.

GENIUSH-CAP			D <sup>2</sup> FOPI-CCS		
Re ( $E_{\text{res}}$ )	Im ( $E_{\text{res}}$ )	Lifetime	Re ( $E_{\text{res}}$ )	Im ( $E_{\text{res}}$ )	Lifetime
1775.8	-0.05	49.6	1775.9	>-0.005	>530.9
1776.7	-0.20	13.1	1777.0	-0.13	20.4
1778.3	-0.41	6.5	1779.8	-0.43	6.2
1809.0	-0.00	178 83.6	1809.0	>-0.0001	>265 460.9
1822.6	-0.06	44.2	1822.6	-0.06	43.5
1832.0	-0.00	4247.4	1832.0	>0	
1834.2	-0.07	40.2	1834.2	>-0.04	>66.4
1835.1	-0.21	12.5	1835.5	-0.13	20.4
1950.4	-0.08	31.5	1950.7	>-0.02	>132.7
1951.4	-0.22	12.1	1951.8	-0.23	11.5
2123.7	-0.12	22.4	2123.6	-0.13	20.4
2124.8	-0.25	10.5	2125.6	-0.22	12.3
2352.5	-0.16	16.6	2352.0	>-0.22	>12.1
2353.8	-0.31	8.6	2354.8	-0.38	7.0
2491.9	-1.10	2.4	2491.9	-0.91	2.9
2602.8	-0.73	3.6	2602.9	-0.87	3.1
2635.1	-0.21	12.6	2635.1	-0.36	7.5
2636.7	-0.38	7.0	2638.0	-0.45	5.9
2642.4	-0.54	4.9	2642.2	-0.58	4.6
2969.6	-0.27	9.8	2969.5	>-0.50	>5.3

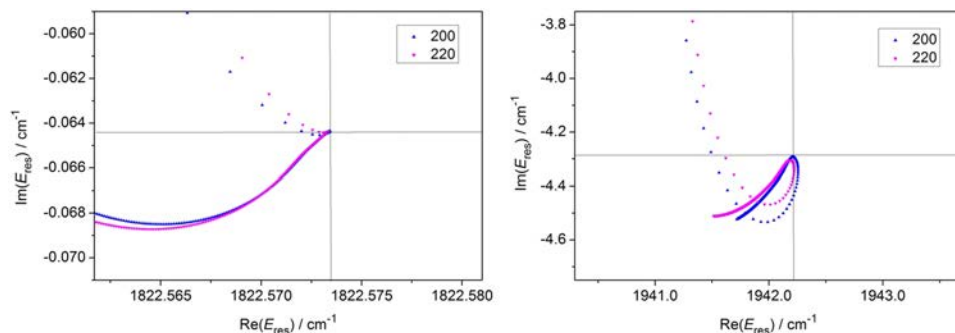


FIG. 1. GENIUSH-CAP eigenvalue trajectories of two selected resonance states of the  $\text{H}_2\text{He}^+$  system, corresponding to the probability density plots of Fig. 2. Blue and pink triangles refer to 200 and 220 basis functions, respectively, along the  $R$  dissociation coordinate in the GENIUSH bound-state computations. Resonance positions (cusps along the trajectories) are indicated by the crossing of the two gray lines.

excited rotational state ( $j = 1$ ), which is estimated within the rigid rotor approximation to be around  $60 \text{ cm}^{-1}$  higher than the first dissociation limit corresponding to the  $j = 0$  state of  $\text{H}_2^+$ . Thus, these states are in fact bound states, as reflected in their extremely long lifetimes. Overall, the close agreement of

the GENIUSH-CAP and  $\text{D}^2\text{FOPI-CCS}$  results proves the correctness of the implementation of the CAP technique within GENIUSH.

In Fig. 1, we present two selected GENIUSH-CAP eigenvalue trajectories, whereby different colors reflect two

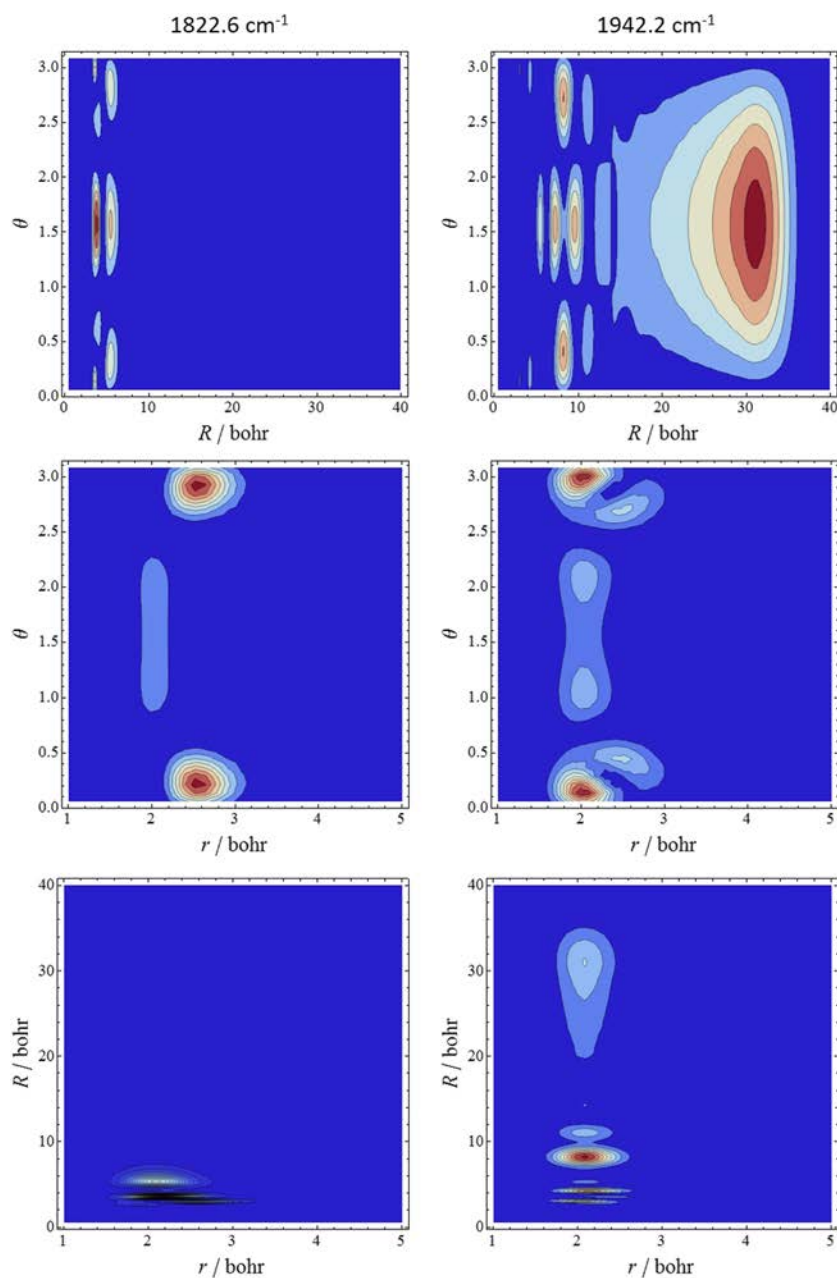


FIG. 2. 2D GENIUSH-CAP probability density plots, see Eq. (9), of two resonance states of  $\text{H}_2\text{He}^+$  corresponding to the resonance energies of Fig. 1. In both cases, the third coordinate is held fixed at its equilibrium value and the CAP is switched on between 30 and 40 bohrs along the  $R$  dissociation coordinate.  $r$  and  $R$  coordinates are given in bohrs, while  $\theta$  is given in radians.

different basis set sizes, 200 and 220 DVR points, used along the  $R$  dissociation coordinate in the bound-state GENIUSH computations. Inspection of the left panel of Fig. 1 reveals that the cusp is very sharp; thus, both the lifetime and the energy of this resonance state can be determined precisely. In contrast, the right panel of Fig. 1 shows a cusp covering a few  $0.1 \text{ cm}^{-1}$  range, yielding a somewhat lower precision. We attribute this behavior to the extent of the delocalization of the resonance states, as discussed below.

### C. Characterizing resonance states with GENIUSH-CAP

Visualization of the resonance probability densities can be useful when the detailed characterization of a resonance state is sought since several important features of the given resonance can be extracted from the nodal structure of the wave function.

Figure 2 depicts three 2D cuts of the probability densities of the two resonance states whose corresponding trajectories are presented in Fig. 1. In each case, the third coordinate is held fixed at its equilibrium value. As shown in the left panels of Fig. 2, the wave function of the resonance state at  $1822.6 \text{ cm}^{-1}$  is localized well inside the potential well along the  $R$  dissociation coordinate. This is supported by the fact that this resonance could be identified even when the CAP was switched on, and thereby the resonance wave function was damped, in the 20–40 bohrs range along  $R$ . In contrast, the dominant part of the wave function corresponding to the resonance state at  $1942.2 \text{ cm}^{-1}$  is extended along the  $R$  coordinate until it is damped by the CAP. Due to this delocalized nature, the  $L^2$  expansion of this resonance state is less effective than that of the previous one. This is probably the reason why its trajectory features a “less sharp” cusp in Fig. 1. The wave function has a significant amplitude in the asymptotic region, indicating that this resonance corresponds to a “less bound” state. This is also reflected in its shorter lifetime compared to the resonance state at  $1822.6 \text{ cm}^{-1}$ . Due to its short lifetime, having an imaginary part of  $-4.3 \text{ cm}^{-1}$ , this state is not listed in Table I.

At the asymptotic region neither resonance states of Fig. 2 are excited in the HH-stretch motion; however, in the case of the resonance state at  $1822.6 \text{ cm}^{-1}$ , one node appears in the  $r$  coordinate at the stronger interaction region of the PES. Additionally, two nodes can be observed along the  $\theta$  coordinate at the interaction region for both resonance states (Fig. 2). This suggests that these states are Feshbach resonances.<sup>3</sup> The  $R$  intermolecular stretching mode is only doubly excited in the case of the  $1822.6 \text{ cm}^{-1}$  resonance state; however, not surprisingly,  $R$  is highly excited for the resonance at  $1942.2 \text{ cm}^{-1}$ .

## IV. A TETRATOMIC TEST CASE: $\text{H}_2 \cdot \text{CO}$

A high-resolution infrared (IR) spectrum measured in the region of the CO fundamental for  $\text{H}_2 \cdot \text{CO}$  was assigned and fully explained by Jankowski *et al.*<sup>8</sup> in 2012, after developing an accurate *ab initio* PES of the complex.<sup>64</sup> Several attempts have been made to understand the resonance energy level structure of this complex, using both sophisticated experimental and theoretical scattering techniques.<sup>65–67</sup>

Employing the GENIUSH-CAP code, we hereby determine numerous rovibrational resonance states of  $\text{H}_2 \cdot \text{CO}$  and analyze them in some detail. This is one of the first cases, to the best of our knowledge, when a four-atomic molecular system is subjected to a variational resonance computation using a model with more than three degrees of freedom.<sup>47–49,68</sup>

### A. Computational details

During the nuclear-motion computations for the  $\text{H}_2 \cdot \text{CO}$  complex, the following masses were used:  $m_{\text{H}} = 1.007\,825\,035 \text{ u}$ ,  $m_{\text{C}} = 12.0 \text{ u}$ , and  $m_{\text{O}} = 15.994\,914\,63 \text{ u}$ . The computations employed a 4D PES, taken from Ref. 64, averaged over the intramonomer vibrations and corresponding to the  $v = 0$  state of CO. The intramonomer distances were fixed at 1.449 and 2.140 bohrs for  $\text{H}_2$  and CO, respectively.<sup>64</sup> The first dissociation limit of  $\text{H}_2 \cdot \text{CO}$  corresponds to the dissociation of the *para*- $\text{H}_2 \cdot \text{CO}$  complex,  $D_{e,para} = 94.096 \text{ cm}^{-1}$  and  $D_{0,para} = 19.440 \text{ cm}^{-1}$ ,<sup>8,64</sup> where the  $\text{H}_2$  product is in its ground rotational state ( $j_1 = 0$ ). The dissociation limit corresponding to *ortho*- $\text{H}_2 \cdot \text{CO}$ ,  $D_{0,ortho}$ , where the  $\text{H}_2$  product is in its first excited rotational state ( $j_1 = 1$ ) is  $2B$  above the *para* dissociation energy within the rigid rotor approximation, where  $B$  refers to the rotational constant of the  $\text{H}_2$  molecule. The GENIUSH computations yield both the *para*- and *ortho*- $\text{H}_2 \cdot \text{CO}$  states in the same computation. The 4D PES implies that the  $B_0$  rotational constant corresponds to the frozen bond length,  $r_0 = 1.449$  bohrs,<sup>64</sup> of the  $\text{H}_2$  unit and thus equals to  $B_0^{\text{PES}} = 56.919 \text{ cm}^{-1}$ . This value is  $2.403 \text{ cm}^{-1}$  lower than the experimental value<sup>69</sup> of  $B_0^{\text{expt}} = 59.322 \text{ cm}^{-1}$ ; therefore, the *ortho* dissociation energy obtained from the reduced-dimensional model,  $113.838 \text{ cm}^{-1}$  relative to the *para* dissociation, is  $4.806 \text{ cm}^{-1}$  lower than the experimental value of the *ortho*- $\text{H}_2 \cdot \text{CO}$  dissociation energy of  $D_{0,ortho}^{\text{expt}} = 118.644 \text{ cm}^{-1}$ . Thus, we expect to obtain *ortho*- $\text{H}_2 \cdot \text{CO}$  energy levels approximately  $5 \text{ cm}^{-1}$  lower (the convergence of certain states may vary) than the absolute energies obtained from experiments.

During the nuclear motion computations, we used generalized Jacobi coordinates, presented in Fig. 3, for the four intermolecular degrees of freedom of the  $\text{H}_2 \cdot \text{CO}$  van der Waals complex. The equilibrium structure of the complex corresponds to  $R_e = 7.9145$  bohrs,  $\theta_{1,e} = 0^\circ$ ,  $\theta_{2,e} = 180^\circ$ , and  $\phi_e = 0^\circ$ . The two intramonomer vibrations are kept frozen during the GENIUSH bound-state computations. In these computations, the following intervals and basis sets are used for the active coordinates:  $R \in [5.0, 40.0]$  bohrs with 200 scaled Laguerre-DVR points,  $\theta_1$  and  $\theta_2 \in (0.0, 180.0)^\circ$  with 30

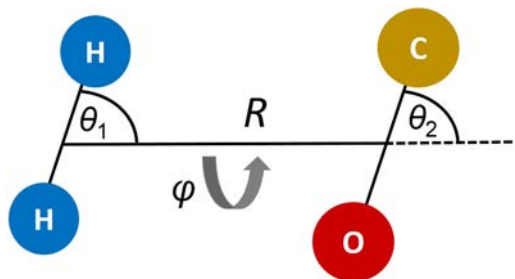


FIG. 3. The coordinate system for the intermolecular degrees of freedom used in the reduced-dimensional GENIUSH computations of  $\text{H}_2 \cdot \text{CO}$ .

unscaled Legendre-DVR points along both coordinates, and  $\phi \in [0.0, 360.0]^\circ$  with 51 Fourier-DVR points. During the GENIUSH-CAP computations, we changed the  $R$  value where the CAP is switched on between 20 and 35 bohrs, while keeping the  $R_{\max}$  value, where the CAP is switched off, fixed at 40 bohrs. We used 220 vibrational GENIUSH eigenvectors as a basis for the CAP computations. Convergence of the resonance states, which usually varies between 0.1 and 1  $\text{cm}^{-1}$ , depending on the given resonance, was tested by changing the number of basis functions on each coordinate by 10%. All the resonance energies are given relative to the *para*-H<sub>2</sub>·CO zero-point energy (ZPE), 74.66  $\text{cm}^{-1}$ , measured with respect to the global minimum of the 4D PES. All three bound states of *para*-H<sub>2</sub>·CO obtained with GENIUSH agree well, within 0.03  $\text{cm}^{-1}$ , with those reported in Ref. 8.

## B. Resonance states of H<sub>2</sub>·CO

In this study, several vibrational resonance states of the H<sub>2</sub>·CO complex have been determined employing the GENIUSH-CAP code and the 4D PES of Ref. 64. Since the first dissociation limit of H<sub>2</sub>·CO, as mentioned above, is  $D_{0,para} = 19.440 \text{ cm}^{-1}$ , in the GENIUSH-CAP computations, one effectively obtains all the states that have an energy higher than  $D_{0,para}$  as resonance states. The dissociation limit corresponding to the *ortho*-H<sub>2</sub>·CO complex, 113.838  $\text{cm}^{-1}$  relative to the *para* dissociation limit and 133.278  $\text{cm}^{-1}$  relative to the *para*-H<sub>2</sub>·CO ZPE in the 4D model, lies much higher than  $D_{0,para}$ . Note also that, as reported in Ref. 8, the ZPE of the *ortho*-H<sub>2</sub>·CO complex is 98  $\text{cm}^{-1}$  relative to the *para* dissociation limit. Thus, all the bound states corresponding to the *ortho*-H<sub>2</sub>·CO complex are expected to be obtained as resonance states with GENIUSH-CAP. In line with this expectation, we found seven extremely long-lived resonance states below the dissociation energy of *ortho*-H<sub>2</sub>·CO.

A joint experimental and theoretical work<sup>8</sup> also reported seven vibrational bound-state energies for *ortho*-H<sub>2</sub>·CO, listed in the third column of Table II. However, the energy levels reported in Ref. 8 were obtained from separate computations for *para*- and *ortho*-H<sub>2</sub>·CO, and the *ortho*-H<sub>2</sub>·CO energies were shifted later with the experimental value of  $D_{0,ortho}^{\text{expt}} = 118.644 \text{ cm}^{-1}$  with respect to the *para* dissociation.

TABLE II. Vibrational resonance energies ( $\text{cm}^{-1}$ ), shifted by 4.8  $\text{cm}^{-1}$ , given relative to the *para*-H<sub>2</sub>·CO zero-point energy ( $p$ -ZPE) (first column), and lifetimes (ns) (second column) of extremely long-lived resonance states of the *ortho*-H<sub>2</sub>·CO complex, obtained from GENIUSH-CAP computations. The third column contains bound vibrational energy levels ( $\text{cm}^{-1}$ ) relative to the  $p$ -ZPE taken from Ref. 8.

GENIUSH-CAP		Reference 8
$E_{\text{res}}$ shifted by 4.8 $\text{cm}^{-1}$	Lifetime	$E_{\text{bound}}$
117.8	7.0	117.8
118.4	1.5	118.6
121.7	3.7	121.7
122.9	1.0	123.1
130.4	3.5	130.5
136.1	4.0	136.3
136.1	2.3	136.4

The GENIUSH-CAP *ortho*-H<sub>2</sub>·CO energy levels therefore deviate by approximately 5  $\text{cm}^{-1}$  from the computed results of Ref. 8. This is the difference between the experimental and the reduced-dimensional theoretical  $D_{0,ortho}$  values.

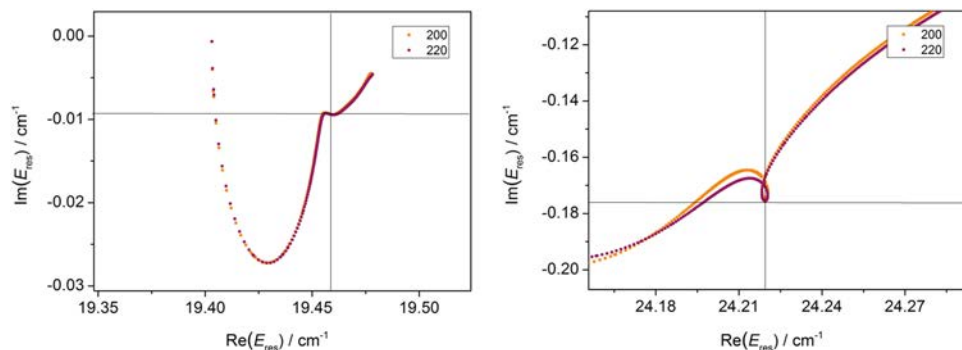
Therefore, if we shift the GENIUSH-CAP resonance energies with the value of the expected difference between the GENIUSH-CAP results and those of Ref. 8, i.e., 4.806  $\text{cm}^{-1}$ , the extremely long-lived GENIUSH-CAP resonance energies agree well, within 0.1–0.3  $\text{cm}^{-1}$ , with the bound *ortho*-H<sub>2</sub>·CO energy levels computed in Ref. 8, see Table II. Lifetimes of these extremely long-lived resonances are also listed in Table II.

In the  $J = 0$  GENIUSH-CAP computations, the rovibrational ground state of *ortho*-H<sub>2</sub>·CO does not appear since it is found in the  $J = 1$  manifold.<sup>8</sup> Seemingly, H<sub>2</sub>·CO belongs to the group of molecules featuring negative “rotational” energies,<sup>70,71</sup> that is, the  $J = 1$  rotationally “excited” ground vibrational state has lower energy than the  $J = 0$  ground vibrational state featuring no rotational “excitation.”

TABLE III. Vibrational resonance energies and lifetimes of the H<sub>2</sub>·CO complex computed with GENIUSH-CAP. The first and the second columns show all resonance positions and lifetimes, respectively, in the range of [ $D_{0,para}$ , 50]  $\text{cm}^{-1}$  with  $|I/2| < 1 \text{ cm}^{-1}$ . The third and fourth columns show energies of the resonance states relative to the first resonance state and to the first resonance states above the new dissociation channels characterized by the rotational energies of CO (boldfaced numbers in the third column), respectively. In the fourth column, relative energies corresponding to resonance states labeled with the  $n$  sequential quantum number are italicized. The fifth column provides assignments ( $j_2$  characterizes the rotation of the CO subunit, see the text for details) of the resonances listed in columns 1 and 2. The sixth and seventh columns show resonance positions and lifetimes, respectively, above the last “bound” *ortho*-H<sub>2</sub>·CO state, up to 145  $\text{cm}^{-1}$ , with  $|I/2| < 1 \text{ cm}^{-1}$ . Resonance positions and lifetimes are given in  $\text{cm}^{-1}$  and ps, respectively.

<i>para</i> -H <sub>2</sub> ·CO					<i>ortho</i> -H <sub>2</sub> ·CO	
Re ( $E_{\text{res}}$ )	Lifetime	$E_{\text{rel},j_2=0}$	$E_{\text{rel},j_2}$	$j_2 n$	Re ( $E_{\text{res}}$ )	Lifetime
19.5	288	0.0	0.0	0 0	136.2	657
20.3	28	0.8	0.8	0 1	136.9 <sup>a</sup>	617
21.8	11	2.4	2.4	0 2	137.0 <sup>a</sup>	583
23.3	82	<b>3.8</b>	0.0	1 0	137.5	48
24.0	7	4.5	0.7	0 3	137.7	36
24.2	15	4.7	0.9	1 1	137.9	6
25.7	10	6.2	2.4	1 2	137.9	30
26.8	4	7.3	3.5		138.6	20
27.8	7	8.3	4.5	1 3	139.2	13
29.6	8	10.1	6.3		139.3	14
31.5	20	<b>12.0</b>	0.0	2 0	139.8	12
31.8	9	12.3	0.3		140.7	4
32.3	12	12.8	0.8	2 1	141.1	7
32.3	12	12.8	0.8		141.2	8
33.7	7	14.2	2.2	2 2	141.9	6
36.1	5	16.6	4.6	2 3	143.7	5
43.2	14	23.7	11.7		143.8	7
43.4	38	<b>23.9</b>	0.0	3 0	144.6	108
44.2	10	24.7	0.8			
44.4	15	24.9	1.0	3 1		
45.8	8	26.3	2.4	3 2		
47.8	5	28.3	4.4	3 3		

<sup>a</sup>One of these resonance states was also reported in Ref. 8.



Two-dimensional probability density plots, see Eq. (9), corresponding to the seven extremely long-lived resonances are presented in the [supplementary material](#). All of the GENIUSH-CAP eigenvalue trajectories of these states cover a very narrow energy range, and the corresponding

eigenvalues could be converged to better than  $0.1 \text{ cm}^{-1}$ . Thus, not surprisingly, the probability density plots of these high-lying resonance states reveal that these states are perfectly localized in the potential well along the  $R$  coordinate. The probability densities show a very clear structure

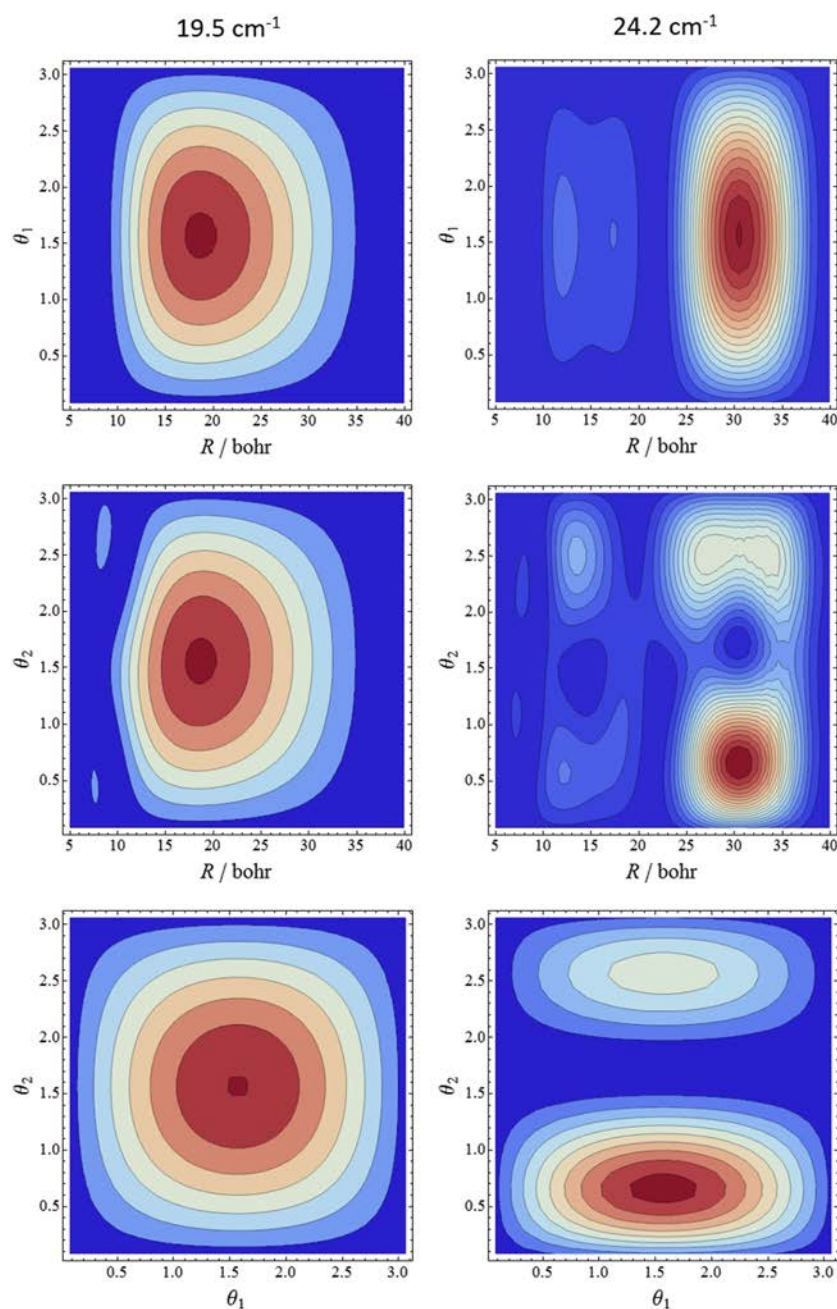


FIG. 5. 2D GENIUSH-CAP probability density plots, see Eq. (9), of two selected resonance states of the  $\text{H}_2\text{-CO}$  complex, with resonance energies of  $19.5$  and  $24.2 \text{ cm}^{-1}$ . The inactive coordinates are held fixed at  $R = 20$  bohrs,  $\theta_1 = 90^\circ$ ,  $\theta_2 = 90^\circ$ , and  $\phi = 180^\circ$  in the case of the resonance at  $19.5 \text{ cm}^{-1}$ , and at  $R = 30$  bohrs,  $\theta_1 = 90^\circ$ ,  $\theta_2 = 45^\circ$ , and  $\phi = 180^\circ$  in the case of the resonance state at  $24.2 \text{ cm}^{-1}$ . The CAP is switched on between 35 and 40 bohrs along the  $R$  dissociation coordinate. The  $R$  coordinate is given in bohrs, while  $\theta_1$  and  $\theta_2$  are given in radians.

implying intermonomer bending excitations. The observed structure is also in line with the fact that the states correspond to the bound states of the *ortho*-H<sub>2</sub>-CO complex.

Note that the appearance of the *ortho*-H<sub>2</sub>-CO bound states as resonances with finite lifetimes is only due to the utilization of the CAP procedure.

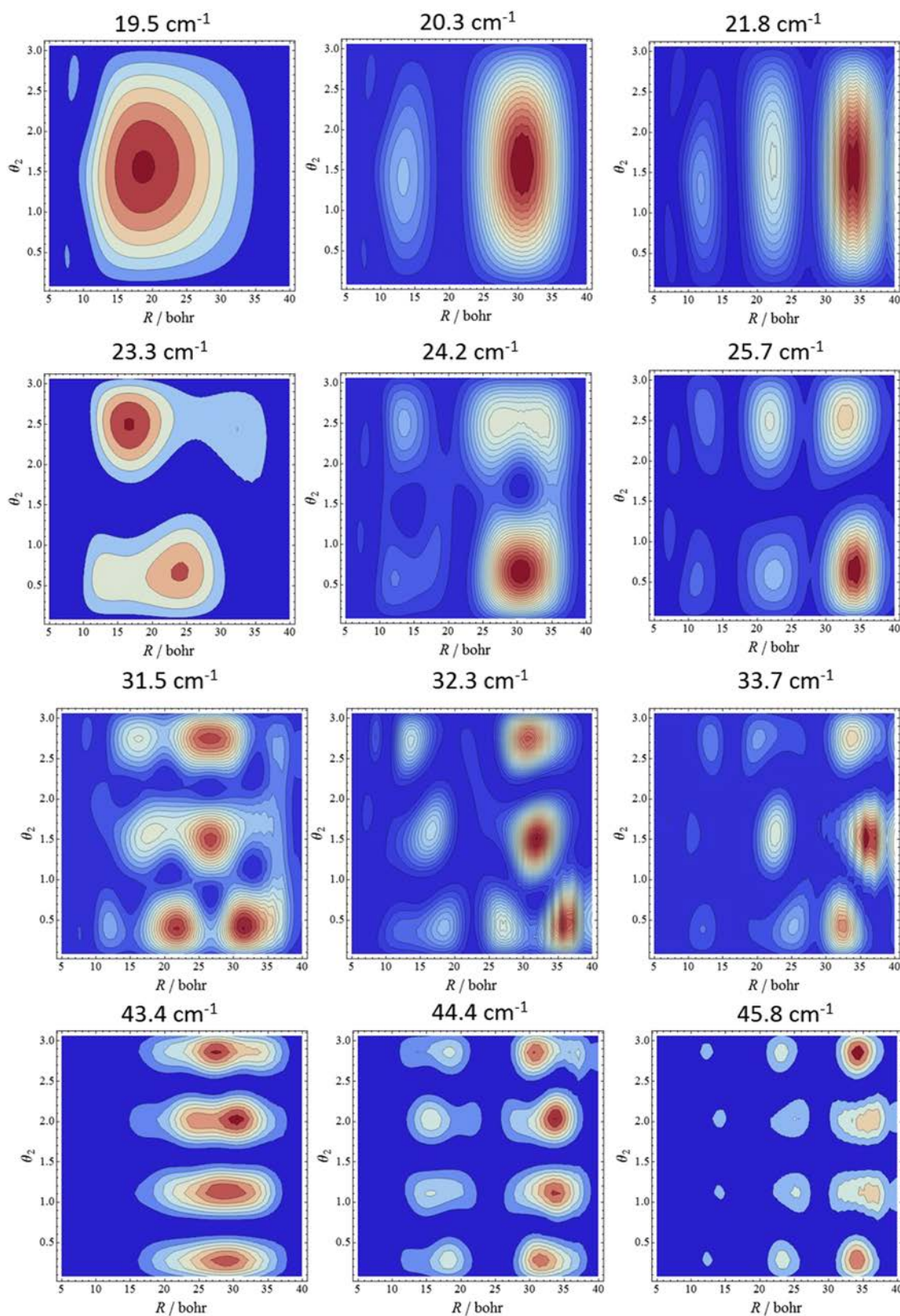


FIG. 6. 2D  $R$ - $\theta_2$  GENIUSH-CAP probability density plots, according to Eq. (9), of 12 selected resonance states of the H<sub>2</sub>·CO complex, with resonance energies of 19.5, 20.3, 21.8, 23.3, 24.2, 25.7, 31.5, 32.3, 33.7, 43.4, 44.4, and 45.8 cm<sup>-1</sup>. The  $\theta_1$  and  $\phi$  coordinates are held fixed at  $\theta_1 = 90^\circ$  and  $\phi = 180^\circ$ . The CAP is switched on between 35 and 40 bohrs along the  $R$  dissociation coordinate. The  $R$  coordinate is given in bohrs, while  $\theta_2$  is given in radians.

We also identified several resonances appearing in the energy region  $[D_{0,para}, 50]$   $\text{cm}^{-1}$ . Energies and lifetimes of these resonance states having  $|\Gamma/2| < 1$   $\text{cm}^{-1}$  are listed in Table III. Figure 4 shows the GENIUSH-CAP eigenvalue trajectories corresponding to two selected resonance states obtained with energies of 19.5  $\text{cm}^{-1}$  and 24.2  $\text{cm}^{-1}$ . Furthermore, in Fig. 5, we present two-dimensional plots, see Eq. (9), of the probability densities of these two resonance states. The resonance state at 19.5  $\text{cm}^{-1}$  (left panels of Fig. 5) is just above the  $D_{0,para}$  limit, with a lifetime as large as 288 ps, and its wave function is localized mainly at 15–25 bohrs. Inspecting the right panels of Fig. 5 reveals that the shorter-lived (15 ps) resonance state at 24.2  $\text{cm}^{-1}$  features a more extended wave function along  $R$ , mainly localized at the asymptotic region of the PES.

In Table III, we also propose assignments for some of the resonance states of *para*- $\text{H}_2\text{CO}$ . The probability density plots of these states are shown in Fig. 6 and more extensively in the [supplementary material](#). In different rows of Fig. 6, a different number of nodes along the  $\theta_2$  coordinate appear in the resonance wave functions, which can be associated with increasing end-over-end rotational excitation of the CO monomer, characterized by the  $j_2$  approximate quantum number. The rotational energies of the CO molecule, estimated within the rigid rotor approximation using the rotational constant  $B_{0,\text{CO}} = 1.9$   $\text{cm}^{-1}$ , are 3.8, 11.4, and 22.8  $\text{cm}^{-1}$  for  $j_2 = 1, 2,$  and  $3$ , respectively. The energies of the leftmost resonances in the rows of Fig. 6, given relative to the energy of the first resonance above  $D_{0,para}$ , are boldfaced in the third column of Table III. These energies coincide with the rigid rotor energies of CO. These

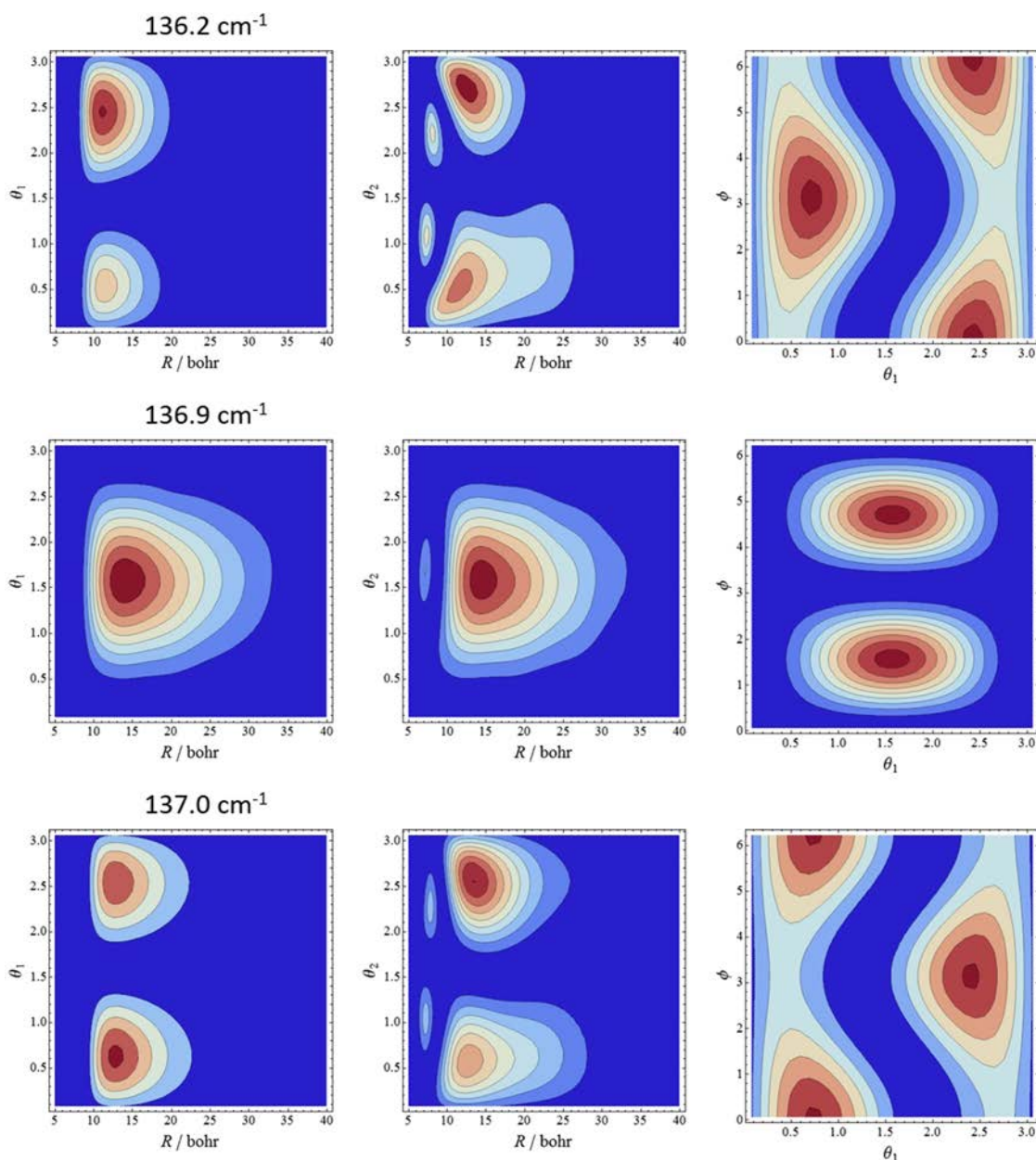


FIG. 7. Selected 2D GENIUSH-CAP probability density plots, according to Eq. (9), of the three longest-lived resonance states of  $\text{H}_2\text{CO}$  above  $D_{0,ortho}$ , with resonance energies of 136.2, 136.9, and 137.0  $\text{cm}^{-1}$ . The other coordinates are held fixed at their equilibrium values. The CAP is switched on between 35 and 40 bohrs along the  $R$  dissociation coordinate. The  $R$  coordinate is given in bohrs, while  $\theta_1$ ,  $\theta_2$ , and  $\phi$  are given in radians.

resonances also exhibit long lifetimes. Thus, the longest-lived resonances at the energies of 19.5, 23.3, 31.5, and 43.4  $\text{cm}^{-1}$  of Table III correspond to the opening of new dissociation channels labeled with  $j_2 = 0, 1, 2,$  and  $3,$  respectively.

Resonance states above the dissociation energy of a given channel characterized by  $j_2$ , shown within the rows of Fig. 6, feature an increasing number of nodes in the  $R$  coordinate. These nodes refer to an increase in the relative kinetic energy of the monomers, which manifests in smaller and smaller wavelength continuum waves describing the asymptotic parts of the resonance wave functions along the  $R$  coordinate. The resonance states corresponding to a given dissociation channel (a given row of Fig. 6) can be labeled with the  $n$  sequential “quantum number” starting from zero for each new  $j_2$  state. The fourth and fifth columns of Table III reveal that the energies of the resonances, labeled with  $n = 1, 2,$  and  $3$  corresponding to a given  $j_2$  quantum number, increase approximately with 0.8, 2.4, and 4.5  $\text{cm}^{-1}$  relative to the energy of the  $n = 0, j_2$  state. Table III also shows that the lifetimes of the resonance states decrease with increasing  $n$ , in line with the delocalization of their wave functions along  $R$ .

The resonance states appearing just above the first dissociation threshold of the  $\text{H}_2\text{-CO}$  complex (first row of Fig. 6) are assigned as Feshbach resonances, as no rotational excitation of CO occurs at the asymptotic region of their wave functions, while near the interaction region, the rotational excitation of CO can be observed. The resonance states appearing just above the new dissociation channels, characterized by  $j_2 = 1, 2,$  and  $3,$  in contrast, seem to be shape resonances, as their wave functions feature the same excitation patterns at the asymptotic and at the interaction regions of the PES.

Between 136 and 137  $\text{cm}^{-1}$ , just above  $D_{0,ortho}$ , we found three long-lived resonance states; their resonance energies and lifetimes are listed in Table III. The probability density plots of the three resonances between 136 and 137  $\text{cm}^{-1}$  are given in Fig. 7 and the supplementary material. These wave-function plots suggest that all three of these resonance states correspond to the *ortho*- $\text{H}_2\text{-CO}$  complex, where both the  $\text{H}_2$  and the CO moieties are in their first rotationally excited states, i.e.,  $j_1 = j_2 = 1$ . However,  $j_1$  and  $j_2$  are only approximate quantum numbers, explaining the small splitting according to the  $m_1$  and  $m_2$  quantum numbers, which are related to the projection of  $\hat{j}_1$  and  $\hat{j}_2$  onto the intermolecular axis connecting the centers of masses of the  $\text{H}_2$  and CO monomers. The  $m_1$  and  $m_2$  quantum numbers are also related to excitations along  $\theta_1$  and  $\theta_2$ , respectively. However, due to the  $J = 0$  constraint, not all the  $3 \times 3 = 9$  possible combinations of  $m_1$  and  $m_2$  can be seen in our computations. The following combinations are feasible (the signs are not assigned):  $m_1 = \pm 1, m_2 = \mp 1$  at the energy of 136.2  $\text{cm}^{-1}$ ,  $m_1 = m_2 = 0$  (no excitations along  $\theta_1$  and  $\theta_2$ ) at 136.9  $\text{cm}^{-1}$ , and  $m_1 = \mp 1, m_2 = \pm 1$  at 137.0  $\text{cm}^{-1}$ .

Our assignments, given in the previous paragraph, are based on energy values and wave-function plots. These assignments were also confirmed by computing overlaps between the resonance wave functions and eigenstates of a simple model system. This assignment technique resembles the coupled rotor decomposition (CRD) analysis introduced in Ref. 72. Briefly, this technique is characterized by the following steps: (i) Using GENIUSH, 3D reduced-dimensional

computations are carried out, in which the  $R$  coordinate is fixed at 80 bohrs and the PES is removed from the Hamiltonian. This results in eigenstates corresponding to two non-interacting rigid monomers,  $\text{H}_2$  and CO, for which quantum number assignment could be easily done based on rigid rotor monomer energies. (ii) Since the 3D computations are carried out on the same DVR grids along the active coordinates as those used during the 4D GENIUSH computations, the resonance wave functions can easily be projected onto the 3D eigenstates. The norm of these projections gives the CRD coefficients. For each resonance state investigated in this study, the  $j_1$  and  $j_2$  approximate quantum numbers could be assigned unambiguously with CRD coefficients usually above 0.9 and always larger than 0.75.

We could also identify an *ortho*- $\text{H}_2\text{-CO}$  resonance state corresponding to the opening of the  $j_2 = 2$  channel at 144.6  $\text{cm}^{-1}$ . The corresponding probability density plot is presented in the supplementary material. Numerous shorter-lived resonance states in the region  $[D_{0,ortho}, 145]$   $\text{cm}^{-1}$  were also found; they are listed in Table III.

## V. SUMMARY AND CONCLUSIONS

This study presents a universal approach to the variational determination of rovibrational resonance states of polyatomic molecules: the complex absorbing potential (CAP) technique<sup>26,27,53,54</sup> has been implemented into the fourth-order<sup>50</sup> quantum chemical quasi-variational nuclear-motion code GENIUSH.<sup>36,38</sup> The GENIUSH-CAP protocol inherits all the advantages of GENIUSH, such as the possibility of computing rovibrational states of molecules of arbitrary size, both in reduced and full dimensions, using arbitrary coordinate systems and embeddings, chosen most suitably for the given system. The GENIUSH-CAP protocol can be employed efficiently for the computation of resonance states of polyatomic molecules and complexes. Furthermore, it has also been shown that inspection of GENIUSH-CAP resonance wave functions facilitates a deeper, qualitative insight into some of the properties of resonance states.

The GENIUSH-CAP code has been validated by comparing the computed resonance energies and lifetimes of the  $\text{H}_2\text{He}^+$  cation to those obtained with the triatomic  $\text{D}^2\text{FOPI-CCS}$  code utilizing the complex coordinate scaling method. The results obtained with the two codes show excellent agreement.

We also report resonance energies and lifetimes for the *ortho* and *para* states of the  $\text{H}_2\text{-CO}$  complex using GENIUSH-CAP. To the best of our knowledge, these are the highest-dimensional variational resonance computations for a four-atomic system. We carried out reduced-dimensional (4D) computations with GENIUSH-CAP, after eliminating the HH and CO stretch coordinates, successfully identified seven long-lived resonances high above the first dissociation limit of the *para*- $\text{H}_2\text{-CO}$  complex, and assigned them to bound states of *ortho*- $\text{H}_2\text{-CO}$ . This assignment is supported by the bound vibrational energy levels reported in Ref. 8 and by the inspection of the GENIUSH-CAP resonance probability density plots. Furthermore, we identified and assigned several vibrational resonances of both *para*- and *ortho*- $\text{H}_2\text{-CO}$  and

discussed the qualitative features of selected states with the help of their probability density plots. Finally, we showed that it is possible to assign approximate quantum numbers to the resonance states obtained with GENIUSH-CAP. This is achieved through computing the projections of the resonance states onto eigenstates of simple model systems, also computed with GENIUSH. In this work, projections onto non-interacting rigid-rotor monomer eigenstates were carried out, resulting in monomer rotational quantum number assignments for the resonance states.

## SUPPLEMENTARY MATERIAL

See [supplementary material](#) for 27 two-dimensional probability density plots, see Eq. (9), obtained from GENIUSH-CAP complex resonance eigenvectors.

## ACKNOWLEDGMENTS

The authors are grateful to NKFIH for financial support (Grant No. K119658).

- <sup>1</sup>M. Born and J. R. Oppenheimer, *Ann. Phys.* **389**, 457 (1927).
- <sup>2</sup>M. Born and K. Huang, *Dynamical Theory of Crystal Lattices* (Oxford University Press, New York, 1954).
- <sup>3</sup>N. Moiseyev, *Non-Hermitian Quantum Mechanics* (Cambridge University Press, New York, 2011).
- <sup>4</sup>A. Carrington, I. R. McNab, and Y. D. West, *J. Chem. Phys.* **98**, 1073 (1993).
- <sup>5</sup>M. Grechko, P. Maksyutenko, T. R. Rizzo, and O. V. Boyarkin, *J. Chem. Phys.* **133**, 139901 (2010).
- <sup>6</sup>N. F. Zobov, S. V. Shirin, L. Lodi, B. C. Silva, J. Tennyson, A. G. Császár, and O. L. Polyansky, *Chem. Phys. Lett.* **507**, 48 (2011).
- <sup>7</sup>T. Szidarovszky and A. G. Császár, *Mol. Phys.* **111**, 2131 (2013).
- <sup>8</sup>P. Jankowski, A. McKellar, and K. Szalewicz, *Science* **336**, 1147 (2012).
- <sup>9</sup>R. B. Bernstein, C. F. Curtiss, S. Imam-Rahajoe, and H. T. Wood, *J. Chem. Phys.* **44**, 4072 (1966).
- <sup>10</sup>W. Shiu, J. J. Lin, and K. P. Liu, *Phys. Rev. Lett.* **92**(10), 103201 (2004).
- <sup>11</sup>Q. Wang, Z. T. Cai, and D. C. Feng, *J. Mol. Struct.: THEOCHEM* **759**, 31 (2006).
- <sup>12</sup>B. Zhang and K. Liu, *J. Chem. Phys.* **122**(10), 101102 (2005).
- <sup>13</sup>R. Otto, J. Ma, A. W. Ray, J. S. Daluz, J. Li, H. Guo, and R. E. Continetti, *Science* **343**, 396 (2014).
- <sup>14</sup>J. D. Tobiason, J. R. Dunlop, and E. A. Rohlfing, *J. Chem. Phys.* **103**, 1448 (1995).
- <sup>15</sup>S. Reid and H. Reisler, *J. Phys. Chem.* **100**, 474 (1996).
- <sup>16</sup>H. Zhang and S. C. Smith, *Phys. Chem. Commun.* **6**, 12 (2003).
- <sup>17</sup>E. F. Vandishoeck, M. C. Vanhemert, A. C. Allison, and A. Dalgarno, *J. Chem. Phys.* **81**, 5709 (1984).
- <sup>18</sup>L. Zhu, K. Suto, J. Fiss, R. Wada, T. Seideman, and R. Gordon, *Phys. Rev. Lett.* **79**, 4108 (1997).
- <sup>19</sup>T. Szidarovszky and K. Yamanouchi, *Phys. Rev. A* **94**(6), 063405 (2016).
- <sup>20</sup>A. Klein, Y. Shagam, W. Skomorowski, P. Zuchowski, M. Pawlak, M. Janssen, N. Moiseyev, S. van de Meerakker, A. van der Avoird, C. Koch, and E. Narevicius, *Nat. Phys.* **13**, 35 (2017).
- <sup>21</sup>A. U. Hazi and H. S. Taylor, *Phys. Rev. A* **1**, 1109 (1970).
- <sup>22</sup>V. A. Mandelshtam, T. R. Ravuri, and H. S. Taylor, *Phys. Rev. Lett.* **70**, 1932 (1993).
- <sup>23</sup>A. Riera, *J. Phys. Chem.* **97**, 1558 (1993).
- <sup>24</sup>J. Tennyson and C. J. Noble, *Comput. Phys. Commun.* **33**, 421 (1984).
- <sup>25</sup>J. Tennyson and B. T. Sutcliffe, *J. Chem. Phys.* **77**, 4061 (1982).
- <sup>26</sup>U. V. Riss and H. D. Meyer, *J. Phys. B* **26**, 4503 (1993).
- <sup>27</sup>H. Mussa and J. Tennyson, *Chem. Phys. Lett.* **366**, 449 (2002).
- <sup>28</sup>V. Ryaboy and N. Moiseyev, *J. Chem. Phys.* **103**, 4061 (1995).
- <sup>29</sup>V. Mandelshtam and N. Moiseyev, *J. Chem. Phys.* **104**, 6192 (1996).
- <sup>30</sup>G. Jolicard, C. Leforestier, and E. J. Austin, *J. Chem. Phys.* **88**, 1026 (1988).
- <sup>31</sup>U. V. Riss and H. D. Meyer, *J. Phys. B* **31**, 2279 (1998).
- <sup>32</sup>J. Tennyson, J. R. Henderson, and N. G. Fulton, *Comput. Phys. Commun.* **86**, 175 (1995).
- <sup>33</sup>J. Tennyson, M. Kostin, P. Barletta, G. Harris, O. Polyansky, J. Ramanlal, and N. Zobov, *Comput. Phys. Commun.* **163**, 85 (2004).
- <sup>34</sup>G. Czako, T. Furtenbacher, A. Császár, and V. Szalay, *Mol. Phys.* **102**, 2411 (2004).
- <sup>35</sup>T. Szidarovszky, A. G. Császár, and G. Czako, *Phys. Chem. Chem. Phys.* **12**, 8373 (2010).
- <sup>36</sup>E. Mátyus, G. Czako, and A. G. Császár, *J. Chem. Phys.* **130**, 134112 (2009).
- <sup>37</sup>E. Mátyus, J. Simunek, and A. G. Császár, *J. Chem. Phys.* **131**, 074106 (2009).
- <sup>38</sup>C. Fábri, E. Mátyus, and A. G. Császár, *J. Chem. Phys.* **134**, 074105 (2011).
- <sup>39</sup>Y. K. Ho, *Phys. Rep.* **99**, 1 (1983).
- <sup>40</sup>J. Xie, B. Poirier, and G. Gellene, *J. Chem. Phys.* **119**, 10678 (2003).
- <sup>41</sup>W. Bian and B. Poirier, *J. Chem. Phys.* **121**, 4467 (2004).
- <sup>42</sup>Y. Xiao and B. Poirier, *J. Chem. Phys.* **122**(12), 124318 (2005).
- <sup>43</sup>Y. Xiao and B. Poirier, *J. Phys. Chem.* **110**, 5475 (2006).
- <sup>44</sup>B. C. Silva, P. Barletta, J. J. Munro, and J. Tennyson, *J. Chem. Phys.* **128**(24), 244312 (2008).
- <sup>45</sup>D. J. Kalita and A. K. Gupta, *J. Chem. Phys.* **133**(13), 134303 (2010).
- <sup>46</sup>D. Lapierre, A. Alijah, R. Kochanov, V. Kokoouline, and V. Tyuterev, *Phys. Rev. A* **94**(4), 042514 (2016).
- <sup>47</sup>M. I. Hernández and D. C. Clary, *J. Chem. Phys.* **101**, 2779 (1994).
- <sup>48</sup>J. M. Bowman and A. Metropoulos, *J. Chem. Soc., Faraday Trans.* **93**, 815 (1997).
- <sup>49</sup>F. N. Dzegilenko and J. M. Bowman, *J. Chem. Phys.* **108**, 511 (1998).
- <sup>50</sup>A. G. Császár, C. Fábri, T. Szidarovszky, E. Mátyus, T. Furtenbacher, and G. Czako, *Phys. Chem. Chem. Phys.* **14**, 1085 (2012).
- <sup>51</sup>E. Mátyus, C. Fábri, T. Szidarovszky, G. Czako, W. D. Allen, and A. G. Császár, *J. Chem. Phys.* **133**, 034113 (2010).
- <sup>52</sup>C. Fábri, E. Mátyus, and A. G. Császár, *Spectrochim. Acta, Part A* **119**, 84 (2014).
- <sup>53</sup>J. Muga, J. Palao, B. Navarro, and I. Egusquiza, *Phys. Rep.* **395**, 357 (2004).
- <sup>54</sup>S. Skokov, J. Bowman, and V. Mandelshtam, *Phys. Chem. Chem. Phys.* **1**, 1279 (1999).
- <sup>55</sup>D. O. Harris, G. G. Engerholm, and W. D. Gwinn, *J. Chem. Phys.* **43**, 1515 (1965).
- <sup>56</sup>A. Dickinson and P. Certain, *J. Chem. Phys.* **49**, 4209 (1968).
- <sup>57</sup>V. Szalay, *J. Chem. Phys.* **99**, 1978 (1993).
- <sup>58</sup>C. Lanczos, *J. Res. Natl. Bur. Stand.* **45**, 255 (1950).
- <sup>59</sup>J. R. Taylor, *Scattering Theory* (Dover, 2006).
- <sup>60</sup>See <http://math.nist.gov/lapack++/> for information about the C++ linear algebra package employed in our work.
- <sup>61</sup>B. Poirier and T. Carrington, *J. Chem. Phys.* **118**, 17 (2003).
- <sup>62</sup>D. De Fazio, *Phys. Chem. Chem. Phys.* **16**, 11662 (2014).
- <sup>63</sup>D. De Fazio, M. de Castro-Vitores, A. Aguado, V. Aquilanti, and S. Cavalli, *J. Chem. Phys.* **137**, 244306 (2012).
- <sup>64</sup>P. Jankowski, L. A. Surin, A. Potapov, S. Schlemmer, A. R. W. McKellar, and K. Szalewicz, *J. Chem. Phys.* **138**(8), 084307 (2013).
- <sup>65</sup>S. Chefdeville, T. Stoecklin, A. Bergeat, K. M. Hickson, C. Naulin, and M. Costes, *Phys. Rev. Lett.* **109**(2), 023201 (2012).
- <sup>66</sup>T. Stoecklin, A. Faure, P. Jankowski, S. Chefdeville, A. Bergeat, C. Naulin, S. B. Morales, and M. Costes, *Phys. Chem. Chem. Phys.* **19**, 189 (2017).
- <sup>67</sup>B. Yang, N. Balakrishnan, P. Zhang, X. Wang, J. M. Bowman, R. C. Forrey, and P. C. Stancil, *J. Chem. Phys.* **145**(3), 034308 (2016).
- <sup>68</sup>Y. Ren, B. Li, and W. Bian, *Phys. Chem. Chem. Phys.* **13**, 2052 (2011).
- <sup>69</sup>K. P. Huber and P. G. Herzberg, *Molecular Spectra and Molecular Structure: IV. Constants of Diatomic Molecules* (Van Nostrand Reinhold, New York, 1979).
- <sup>70</sup>J. Sarka, C. Fábri, T. Szidarovszky, A. G. Császár, Z. Lin, and A. B. McCoy, *Mol. Phys.* **113**, 1873 (2015).
- <sup>71</sup>J. Sarka and A. G. Császár, *J. Chem. Phys.* **144**, 154309 (2016).
- <sup>72</sup>J. Sarka, A. G. Császár, and E. Mátyus, *Phys. Chem. Chem. Phys.* **19**, 15335 (2017).